Ionics (2015) 21:1081–1088
DOI 10.1007/s11581-014-1277-y

ORIGINAL PAPER

Electrochemical studies on novel films consisting of phosphorus-doped multi-walled carbon nanotubes

Nikos G. Tsierkezos · Paweł Szroeder · Robert Fuge · Uwe Ritter

Received: 29 July 2014 / Revised: 5 September 2014 / Accepted: 27 September 2014 / Published online: 10 October 2014

Abstract Films consisting of phosphorus-doped multi-walled carbon nanotubes (further denoted as P-MWCNTs) were fabricated by means of chemical vapor deposition technique with decomposition of triphenylphosphine in the presence of catalyst. The P-MWCNTs films were characterized using scanning electron microscopy, transmission electron microscopy, and Raman spectroscopy. The P-MWCNTs films were electrochemically investigated with respect to their response to ferrocyanide/ferricyanide, $[Fe(CN)_6]^{3-/4-}$ by means of cyclic voltammetry and electrochemical impedance spectroscopy techniques. The findings reveal that the phosphorus-doping of nanotubes improves their electrochemical response, but it cannot compete the nitrogen-doping of nanotubes, that enhances even more the sensitivity and detection ability of carbon nanotubes. Specifically, the limit of detection of P-MWCNTs towards $[Fe(CN)_6]^{3-/4-}$ (LOD=1.0 μM) lies between those obtained for pristine MWCNTs (LOD=1.57 μM) and nitrogen-doped MWCNTs (LOD=0.47 μM). The findings exhibit the important role which plays the doping of carbon nanotubes with elements for the improvement of their electrocatalytic properties.

N. G. Tsierkezos (✉) · U. Ritter
Department of Chemistry, Institute of Chemistry and Biotechnology, Ilmenau University of Technology, Weimarer Straße 25, 98693 Ilmenau, Germany
e-mail: nikos.tsierkezos@tu-ilmenau.de

P. Szroeder
Institute of Physics, Faculty of Physics, Astronomy and Informatics, Nicolaus Copernicus University, Grudziadzka 5, 87-100 Toruń, Poland

R. Fuge
Leibniz Institute for Solid State and Materials Science Research, Helmholtzstraße 20, 01069 Dresden, Germany

Keywords Electrochemical studies · Multi-walled carbon nanotubes · Phosphorus-doped carbon nanotubes · Raman spectroscopy · Electron microscopy

Introduction

Multi-walled carbon nanotubes (further denoted as MWCNTs) are considered very promising and attractive nanomaterials for various applications in electroanalysis due to their marvelous electrical, chemical, and mechanical properties [1–5]. Consequently, MWCNTs were widely used for the fabrication of composite electrodes and the construction of precise electrochemical devices since they enhance the electron transfer rate and the sensitivity of sensing systems, due to their large surface area and their high electrical conductivity [6, 7]. According to literature reports, novel composite electrodes based on MWCNTs were extensively applied with great electrochemical performance for the electroanalysis of various redox systems of great interest [8–10]. The nanotube curvature changes the chemically inert graphite surface and makes it quite easier to incorporate elements on the tube surface. In this context, nitrogen, which is known to have low doping levels in bulk graphite, can be easily incorporated into the structure of carbon nanotubes by substitution. It is well known that inclusion of non-carbon atoms into the hexagonal network of carbon nanotubes modifies the electronic and chemical properties due to variations in electronic structure [11]. Nitrogen, for example, acts as an electron donor in carbon nanotubes since it has five valence electrons, causing a shift in the Fermi level to the conduction bands, and hence making all nitrogen-doped tubes metallic, regardless of their geometry. Nitrogen can also be incorporated within carbon nanotubes in a pyridine-like fashion [12]. It is noteworthy that the doped sites within carbon nanotubes significantly modify chemical reactivity, thereby broadening the spectrum of their

possible applications, especially in the field of electrochemical sensing. It was recently found that phosphorus can be effectively incorporated into carbon nanotubes either as single substitution dopant [13] or as co-dopant along with nitrogen [14]. Theoretical investigations showed that both phosphorus and phosphorus-nitrogen defects are characterized by the presence of highly localized state close to the Fermi level, a promising evidence for notorious chemical reactivity and electrochemical sensing capabilities [15]. The aim of the present research work is the fabrication of phosphorus-doped carbon nanotubes and their spectroscopic and electrochemical characterization. Specifically, phosphorus-doped multi-walled carbon nanotubes (further denoted as P-MWCNTs) were successfully fabricated by means of chemical vapor deposition (CVD) technique with decomposition of triphenylphosphine (TPP) onto oxidized silicon substrate (Si/SiO_2) in the presence of ferrocene ($FeCp_2$) that served as catalyst. The P-MWCNTs films were characterized by means of scanning electron microscopy (SEM), transmission electron microscopy (TEM), and Raman spectroscopy. Furthermore, the electrochemical response of P-MWCNTs towards the standard redox system ferrocyanide/ferricyanide, $[Fe(CN)_6]^{3-/4-}$ was studied by means of cyclic voltammetry (CV) and electrochemical impedance spectroscopy (EIS) techniques in aqueous KCl solution (1.0 M). For comparison reasons electrochemical studies of $[Fe(CN)_6]^{3-/4-}$ on pristine undoped multi-walled carbon nanotubes (further denoted as MWCNTs) and nitrogen-doped multi-walled carbon nanotubes (further denoted as N-MWCNTs) were also performed. The findings are fairly promising and demonstrate the important role which plays the doping of carbon nanotubes with elements for the improvement of their electrochemical response.

Experimental

Chemicals and solutions

Triphenylphosphine (>99 %), ferrocene (>98 %), and cyclohexane (>99 %), used for the fabrication of P-MWCNTs, were purchased from Sigma-Aldrich. Potassium hexacyanoferrate(III), (>99.0 %), potassium hexacyanoferrate(II) trihydrate, (>98.5 %), and potassium chloride (>99.0 %), used for the electrochemistry experiments, were purchased from Sigma-Aldrich. All chemicals were used as received without any further purification. For the electrochemistry measurements, a stock solution of $K_3Fe(CN)_6/K_4Fe(CN)_6$ mixture (1.0 mM) was prepared by dissolving the appropriate amounts of the salts in 1.0-M aqueous KCl solution. The stock solution was prepared immediately prior to the electrochemical experiments by using high-quality distilled water having a specific conductivity of less than 0.1 $\mu S \cdot cm^{-1}$. The measured solutions, in the concentration range from 0.032–0.250 mM, were prepared directly in the electrochemical cell with progressive addition of appropriate volume of the stock solution in 1.0-M aqueous KCl solution. The experiments were carried out at the room temperature.

Fabrication of P-MWCNTs films

The fabrication of P-MWCNTs was carried out successfully by means of CVD technique with decomposition of TPP (phosphorus source material) in cyclohexane (carbon source material) onto silicon/silicon oxide substrate in the presence of $FeCp_2$ (catalyst). The concentration of ferrocene was fixed at 2.0 wt%, since high quality carbon nanotubes were previously obtained using the same experimental conditions [16, 17]. The concentration of TPP, the source of phosphorus atoms, was fixed at 1.0 wt%. For the growth process, 4.0 mL of TPP/$FeCp_2$ mixture in cyclohexane was introduced to the furnace at the temperature of 900 °C through a syringe with flow rate of 0.2 mL min^{-1} (the growth processing time was fixed at 20 min). The scheme of the CVD apparatus and experimental details concerning the pyrolysis technique were already reported in previous published articles [18, 19]. In order to construct the working electrode for the electrochemistry measurements, the MWCNT-based film produced was connected to platinum wire by using silver conducting coating. Once the silver coating was dried (after 24 h), the silver conducting part of the electrode was fully covered with varnish protective coating [20].

Apparatus and experiments

All the electrochemical measurements were performed on electrochemical working station Zahner (IM6/6EX, Germany). The obtained results were analyzed by means of Thales software (version 4.15). A three electrode system consisting of either pristine MWCNTs, P-MWCNTs, or N-MWCNTs working electrode, platinum auxiliary electrode, and Ag/AgCl (saturated KCl) reference electrode was used for the electrochemistry measurements. The electrochemical impedance spectra were recorded in the frequency range from 0.1 to 100 kHz at the half-wave potential of the studied redox system $[Fe(CN)_6]^{3-/4-}$ ($E_{1/2}$=+0.271 V vs. Ag/AgCl). All experiments were carried out at the room temperature. In all electrochemistry measurements, the solutions were deoxygenated by purging with high-purity nitrogen. More details regarding the electrochemistry measurements were already reported in previous published articles [21–23]. The morphology and elemental composition of P-MWCNTs films were examined by transmission electron microscope (TECNAI, Philips) and scanning electron microscope (XL30 ESEM, FEI/Philips) equipped with an energy dispersive X-ray

spectrometer [24]. Raman spectra of pristine MWCNTs, P-MWCNTs, and N-MWCNTs films were recorded using inVia microprobe spectrometer (Renishow, Gloucestershire, UK), which was coupled to Leica confocal microscope. Laser excitation light of the length of 488 nm and power of about 100 mW was used. The diameter of the laser spot was about 1 μm. The main Raman modes characteristic to sp^2-carbon materials were fitted using Lorentzian curves.

Results and discussion

Scanning electron microscopic and transmission electron microscopic analysis

Representative SEM and TEM images obtained for P-MWCNTs are shown in Fig. 1. SEM analysis of P-MWCNTs demonstrates the presence of corrugated carbon nanotubes that are obviously shorter compared to either the pristine undoped MWCNTs (the nanotubes are quite large and straight) or N-MWCNTs (the nanotubes are large and bamboo-shaped) [25]. Independent of the concentration of TPP used in the precursor solution, all produced phosphor-doped nanotubes are corrugated and are obviously smaller than MWCNTs and N-MWCNTs. Furthermore, the SEM images exhibit that the P-MWCNTs are almost free of amorphous carbon. The TEM images of P-MWCNTs reveal that the nanotubes have uniform distribution in diameter with outer diameter in the range of 80–100 nm. In addition, the presence of residue catalytic iron nanoparticles distributed at the tips and inside the carbon nanotubes can be clearly observed in recorded TEM micrographs. The encapsulated iron nanoparticles have rod shape and their size reaches about 200 nm in length. The presence of doped-phosphorus along with iron nanoparticles favors the formation of several compounds. Consequently, probably during the progressive catalytic growing of P-MWCNTs, formation of oxidized iron and iron phosphorus compounds takes place. To study the chemical composition of P-MWCNTs arrays, EDS measurements were performed on the areas selected randomly from P-MWCNTs films. As was expected, the growth of carbon nanotubes with decomposition of triphenylphosphine leads to incorporation of large number of phosphorus atoms into the structure of carbon nanotubes (about ~2 %).

Raman spectroscopic analysis

The Raman spectra recorded for MWCNTs, N-MWCNTs, and P-MWCNTs are displayed in Fig. 2. Three main Raman modes, G, G', and D, which are characteristic to the sp^2 carbons, are well resolved. The parameters of the main Raman features for all three different types of carbon nanotubes are reported in Table 1, for comparison reasons. At

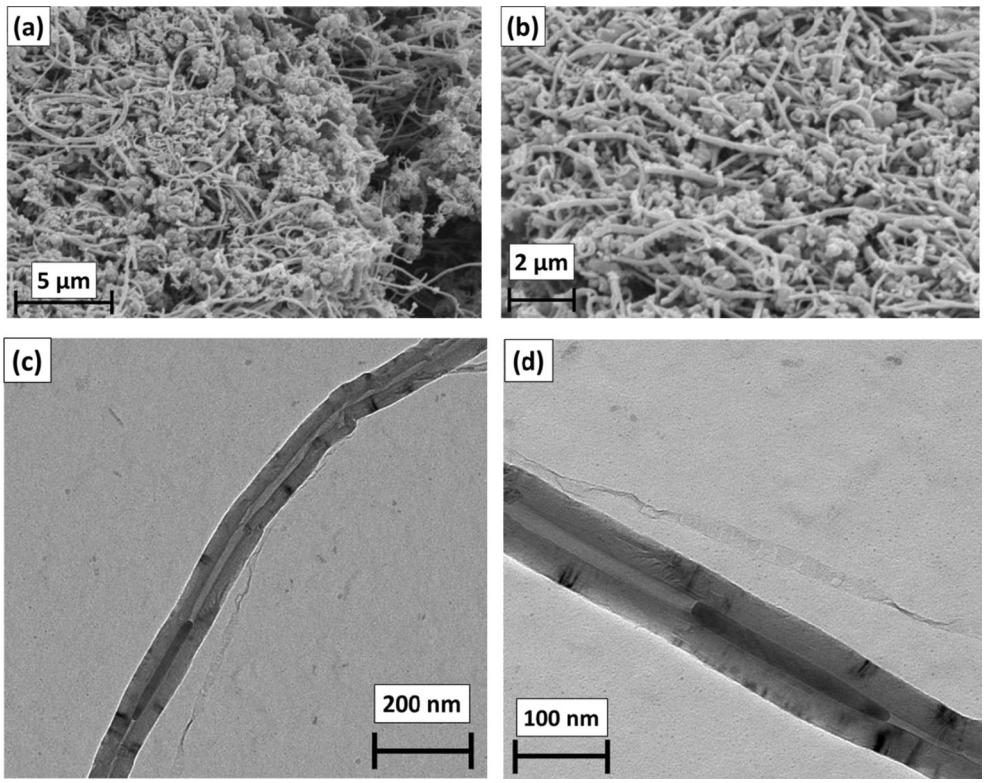

Fig. 1 SEM (**a**, **b**) and TEM (**c**, **d**) micrographs taken for P-MWCNTs. The SEM images were taken with accelerating voltage of 10 kV and magnification factors of 5000 (**a**) and 8000 (**b**)

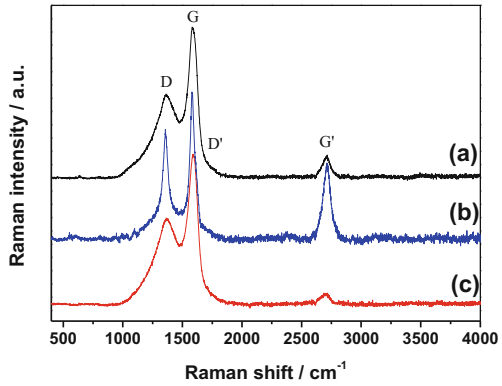

Fig. 2 Raman spectra recorded for pristine MWCNTs (**a**), N-MWCNTs (**b**), and P-MWCNTs (**c**) films

1588.14 cm^{-1} appears symmetry allowed G mode, which was slightly up-shifted to the value 1588.83 cm^{-1} in nanotubes doped with phosphorus, whereas significant down-shift is observed in carbon nanotubes containing nitrogen. The G mode has its second order counterpart, G', at ~2700 cm^{-1}. Its integral intensity is weaker in carbon nanotubes doped with phosphorus than in the pristine MWCNTs. On the other hand, introduction of nitrogen into the tubular walls causes significant increase of the relative intensity of G' band. In Raman spectra of both pristine MWCNTs and P-MWCNTs relatively strong disorder induced D-mode appears. It has been shown that, the relative intensity of D and G lines, as well as G' and G lines is a measure of disorder and number of graphene layers in low dimensional carbons [26–29]. The intensity ratio of D and G bands, I_D/I_G, is a little higher in P-MWCNTs and N-MWCNTs, proving higher disorder in the doped carbon material. Using the procedure, which was already described in our previously published work [30], the average distance between defects can be estimated to 13.5±0.2 nm, 12.3±0.2 nm and 13.1±0.2 nm for pristine MWCNTs, N-MWCNTs, and P-MWCNTs, respectively.

Electrochemical analysis

Representative CVs recorded for $[Fe(CN)_6]^{3-/4-}$ (1.0 M KCl) on P-MWCNTs composite film at the scan rate of 0.02 V s^{-1} showing the effect of the change of concentration of redox system in the concentration range of 0.032–0.250 mM are shown in Fig. 3a. The change of the anodic current response of P-MWCNTs composite film with the variation of the concentration of $[Fe(CN)_6]^{3-/4-}$ is presented graphically in Fig. 3b. The estimated electrochemical parameters of $[Fe(CN)_6]^{3-/4-}$ on P-MWCNTs film are presented in Table 2 along with those obtained under the same conditions for $[Fe(CN)_6]^{3-/4-}$ on pristine undoped MWCNTs and N-MWCNTs, for comparison reasons. As it can be seen in CVs shown in Fig. 3a, on P-MWCNTs, a pair of well-defined reversible redox waves lying at about E_p^{ox}≈0.306 V (vs. Ag/AgCl) and E_p^{red}≈0.236 V (vs. Ag/AgCl) can be observed during the anodic and cathodic scans, respectively, corresponding to the one-electron transfer process involving the standard redox system $[Fe(CN)_6]^{3-/4-}$. The half-wave potential of $[Fe(CN)_6]^{3-/4-}$ on P-MWCNTs film, estimated as the average value of the oxidation and reduction potentials, lies at about $E_{1/2}$≈0.271 V (vs. Ag/AgCl) and is almost similar within experimental error to that measured on either pristine undoped MWCNTs ($E_{1/2}$≈0.271 V vs. Ag/AgCl) or N-MWCNTs ($E_{1/2}$≈0.271 V vs. Ag/AgCl) films. This finding was expectable and confirms that the $E_{1/2}$ for reversible redox systems is independent on working electrode's material. The recorded CVs illustrate that the investigated redox couple $[Fe(CN)_6]^{3-/4-}$ appears to be reversible on P-MWCNTs film. Namely, the CVs recorded on this particular electrode are quite symmetric and the peak current ratio of reverse and forward scans is equal to unity and is independent of scan rate demonstrating that there are no parallel chemical reactions coupled to the electrochemical process (it is well known that such reactions can significantly alter the ratio of peak currents). Furthermore, the oxidative and reductive peak currents are essentially constant for several cycles (no loss of electro-activity was observed for recording continuously 50 cycles). This finding demonstrates that there are no chemical reactions coupled to the electron transfer and that the involved electro-active species $[Fe(CN)_6]^{3-/4-}$ are stable in the time frame of the experiment confirming, thus, that the charge-transfer process occurring on P-MWCNTs film is reversible. It must be mentioned that similar behavior was observed for $[Fe(CN)_6]^{3-/4-}$ onto pristine MWCNTs and N-MWCNTs films. The effect of variation of scan rate on oxidation peak current of $[Fe(CN)_6]^{3-/4-}$ on P-MWCNTs film shows a linear variation of peak current with the square root of scan rate indicating that the electrochemical process occurring on P-MWCNTs is diffusion controlled (this is another evidence of the reversibility of investigated $[Fe(CN)_6]^{3-/4-}$

Table 1 Positions of D, G, and G' Raman bands, intensity ratios of D and G bands (I_D/I_G), and integral intensity ratios of G' and G bands ($A_{G'}/A_G$) for pristine MWCNTs, N-MWCNTs, and P-MWCNTs films

Material	$\tilde{\nu}_D$ /cm^{-1}	$\tilde{\nu}_G$	$\tilde{\nu}_{G'}$	I_D/I_G	$A_{G'}/A_G$
MWCNTs	1364.3±0.5	1588.14±0.15	2708.4±0.8	0.548±0.007	0.125±0.004
N-MWCNTs	1357.7±0.4	1584.01±0.18	2712.0±0.4	0.651±0.011	0.697±0.011
P-MWCNTs	1366.4±0.5	1588.83±0.16	2697±2	0.580±0.008	0.082±0.004

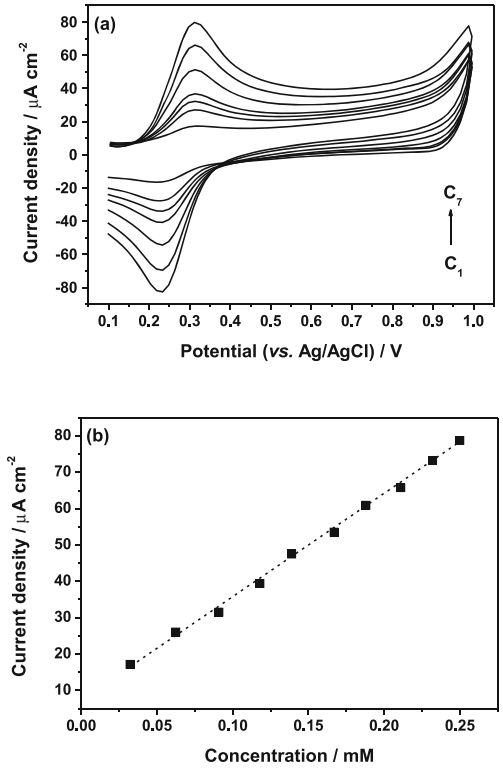

Fig. 3 (**a**) Representative CVs recorded for various concentrations of $[Fe(CN)_6]^{3-/4-}$ (1.0 M KCl) on P-MWCNTs film at the scan rate of 0.02 V s^{1} (the CVs from inner to outer correspond to the following concentrations: 0.032, 0.063, 0.091, 0.118, 0.167, 0.211, and 0.250 mM); (**b**) Variation of oxidation peak current with the concentration of $[Fe(CN)_6]^{3-/4-}$ in the concentration range of 0.032–0.250 mM

system onto P-MWCNTs film). Similarly, the studied system $[Fe(CN)_6]^{3-/4-}$ appears to be diffusion controlled onto pristine MWCNTs and N-MWCNTs. The values of anodic and cathodic peak potential separation ($\Delta E_p = E_p^{ox} - E_p^{red}$) obtained for $[Fe(CN)_6]^{3-/4-}$ on P-MWCNTs film appear to be slightly dependent on concentration (they increase slightly with concentration) and lie in the range from 0.070 to 0.077 V in the concentration range of 0.032–0.250 mM, are slightly greater compared to the ideal value of $\Delta E_p = 0.059$ V [31], which is indicative of reversible one-electron transfer redox process. It must be mentioned that the observed slight dependence of ΔE_p on concentration of redox system can be attributed to uncompensated resistance effect. It is, however, very interesting that the ΔE_p value of about 0.070 V obtained for $[Fe(CN)_6]^{3-/4-}$ on P-MWCNTs film lies between those obtained for the same redox system onto pristine undoped MWCNTs ($\Delta E_p \approx 0.084$ V) and N-MWCNTs ($\Delta E_p \approx 0.064$ V) composite films. Considering that the ΔE_p varies inversely with the heterogeneous electron transfer rate constant (k_s), and thus, with the kinetics of charge-transfer process occurring onto electrode's surface, it can be concluded that the doping of carbon nanotubes with phosphorus diminishes the ΔE_p value (for about 14 mV), and thus, it improves the kinetics of redox reaction. It is, moreover, obvious that the nitrogen-doping of nanotubes decreases even more the ΔE_p value (for about 20 mV) and improves further the kinetic of redox system. The k_s values were estimated by means of electrochemical absolute rate relation that is based on degree of peak separation between the forward and reverse scans. Namely, in order to determine the heterogeneous electron transfer rate constants of $[Fe(CN)_6]^{3-/4-}$ on P-MWCNTs, the procedure suggested in literature by Nicholson [32], which relates k_s with ΔE_p through a working curve of dimensionless kinetic parameter ψ, was applied. For the determination of k_s, the diffusion coefficient of $[Fe(CN)_6]^{3-/4-}$ was taken as $D = 7.2 \times 10^{-6}$ $cm^2 s^{-1}$ [33]. The determined k_s values of $[Fe(CN)_6]^{3-/4-}$ on P-MWCNTs film are included in Table 2 along with those estimated for $[Fe(CN)_6]^{3-/4-}$ on pristine undoped MWCNTs and N-MWCNTs films for comparison reasons. The findings demonstrate that the kinetics of redox process onto P-MWCNTs is faster compared to that occurring onto pristine undoped MWCNTs film (about 66 % faster). Furthermore, the kinetics of $[Fe(CN)_6]^{3-/4-}$ onto P-MWCNTs film appears to be slower compared to that taking place onto N-MWCNTs (about 44 % slower) film. The findings clearly exhibit that the phosphor-doping improves somehow the kinetics of redox process occurring onto carbon nanotubes.

Table 2 Anodic peak potential (E_p^{ox}), cathodic peak potential (E_p^{red}), half-wave potential ($E_{1/2}$), anodic and cathodic peak potential separation (ΔE_p), anodic and cathodic peak current ratio (i_p^{ox}/i_p^{red}), heterogeneous electron transfer rate constant (k_s), charge transfer resistance (R_{ct}), lower limit of detection (*LOD*), and sensitivity (*S*) for pristine MWCNTs, N-MWCNTs, and P-MWCNTs composite films towards $[Fe(CN)_6]^{3-/4-}$ (1.0 M KCl)

Parameters	Pristine MWCNTs	N-MWCNTs	P-MWCNTs
E_p^{ox}/V[a]	0.313	0.303	0.306
E_p^{red}/V[a]	0.229	0.239	0.236
$E_{1/2}$/V[a,b]	0.271	0.271	0.271
ΔE_p/V	0.084	0.064	0.070
i_p^{ox}/i_p^{red}/A	1.01	1.00	1.01
$k_s/10^{-3}$ cm s^{-1}[c]	9.0	26.9	14.98
R_{ct}/Ω[d]	50	17	35
LOD/μM[e]	1.57	0.47	1.00
S/A M^{-1} cm^{-2}	0.423	0.540	0.499

[a] All potentials are reported with respect to the Ag/AgCl (KCl sat.) reference electrode

[b] The $E_{1/2}$ values were determined as the average values of E_p^{ox} and E_p^{red}

[c] The k_s values were determined from electrochemical absolute rate relation: $\psi = (D_o/D_R)^{a/2} k_s (n\pi F v D_o/RT)^{-1/2}$, where ψ is kinetic parameter, a the charge transfer coefficient ($a \approx 0.5$), D_o, D_R the diffusion coefficients of oxidized and reduced species, respectively ($D_o \approx D_R$), and n the number of electrons involved in the redox reaction ($n = 1$)

[d] The EIS parameters were determined by using the equivalent electrical circuit ($R_s + (C_{dl}/(R_{ct} + Z_w))$) (software Thales, version 4.15)

[e] The lower limits of detection were estimated on the basis of signal-to-noise (*S*/*N*) ratio of 3

However, the phosphor-doping cannot compete the nitrogen-doping that improves even more the charge-transfer kinetics of the process taking place onto carbon nanotubes. These findings confirm the particularly enhanced electrocatalytic properties of carbon nanotubes that incorporate nitrogen atoms into their structure [34, 35]. In order to estimate the detection ability and sensitivity of P-MWCNTs film towards $[Fe(CN)_6]^{3-/4-}$ the variation of oxidation peak current with the concentration of redox system was studied. The findings demonstrate that the P-MWCNTs film exhibits linear voltammetric response towards $[Fe(CN)_6]^{3-/4-}$ in the investigated concentration range of 0.032–0.250 mM (Fig. 3b). From the linear concentration-current calibration curve, the detection limit and sensitivity of P-MWCNTs towards $[Fe(CN)_6]^{3-/4-}$ were estimated as 1.0 μM and 0.499 A M^{-1}, respectively. It is very interesting that the limit of detection determined for P-MWCNTs towards $[Fe(CN)_6]^{3-/4-}$ lies between those estimated for pristine undoped MWCNTs (LOD=1.57 μM) and N-MWCNTs (LOD=0.47 μM) films towards the same redox system $[Fe(CN)_6]^{3-/4-}$ [36]. Accordingly, the sensitivity of pristine undoped MWCNTs film and the films consisting of either phosphorus-doped or nitrogen-doped carbon nanotubes tend to increase with the following order: MWCNTs (0.423 A M^{-1} cm^{-2})<P-MWCNTs (0.499 A M^{-1} cm^{-2})<N-MWCNTs (0.540 A M^{-1} cm^{-2}) (Table 2). It is very interesting that with the same order increases the kinetic parameter k_s of $[Fe(CN)_6]^{3-/4-}$, indicating that the doping of nanotubes with elements improves their electrocatalytic properties.

It would be very interesting to compare the limit of detection of P-MWCNTs towards $[Fe(CN)_6]^{3-/4-}$ with those reported in the literature for other novel composite films. It is quite remarkable that our novel P-MWCNTs film exhibits greater detection capability towards the redox couple $[Fe(CN)_6]^{3-/4-}$ compared to the other novel films reported in literature. For instance, Perenlei et al. [37] reported that the detection limits of glassy carbon electrode modified with MWCNTs and titanium dioxide towards $[Fe(CN)_6]^{3-/4-}$ estimated at the scan rates of 0.10 V s^{-1} and 0.005 V s^{-1} were LOD=48.6 μM and LOD=1.10 μM, respectively, which appear to be significantly poorer compared to that estimated in the present work at the scan rate of 0.02 V s^{-1} for novel P-MWCNTs composite film towards the same redox system (LOD=1.0 μM). Furthermore, Pandurangachar et al. [38] reported that the detection limit of carbon paste electrode modified with 1-butyl 4-methylpyridinium tetrafluoro borate towards $[Fe(CN)_6]^{3-/4-}$ is about 100 μM, which is considerably poorer compared to that estimated for P-MWCNTs towards the same redox system in the present work (LOD=1.0 μM). Besides, the detection limit of carbon paste electrode modified with sodium dodecyl sulfate towards $[Fe(CN)_6]^{3-/4-}$ of about 100 μM, reported by Niranjana et al. [39], appears to be also significantly poorer compared to that obtained for $[Fe(CN)_6]^{3-/4-}$ on our novel P-MWCNTs composite film (LOD=1.0 μM). In addition, Hirano et al. [40] reported a detection limit of 30 μM for glass capillary ultra-microelectrode towards the couple $[Fe(CN)_6]^{3-/4-}$ that is as well noticeably poorer compared to that estimated for P-MWCNTs film towards $[Fe(CN)_6]^{3-/4-}$ in the present work (LOD=1.0 μM). A comparison of the low limits of detection of undoped MWCNTs, P-MWCNTs, N-MWCNTs with those of other novel composite films published in literature is shown in histograms in Fig. 4. This comparison clearly demonstrates that the detection ability of our novel P-MWCNTs composite film appears to be significantly improved compared to that of other composite films reported in literature. These findings exhibit the excellent electrocatalytic performance of P-MWCNTs composite film.

The electrochemical behavior of redox system $[Fe(CN)_6]^{3-/4-}$ on novel P-MWCNTs composite film was further investigated by means of EIS technique. Representative EIS spectra recorded for various concentrations of $[Fe(CN)_6]^{3-/4-}$ on P-MWCNTs composite film in the concentration range of 0.032–0.250 mM are displayed in Fig. 5a. A zoom of EIS spectra in high-frequency range is shown in Fig. 5b. In EIS spectra, which are graphically displayed as Nyquist plots, the complex impedance of the studied system is presented as the sum of the real (Z_{re}) and

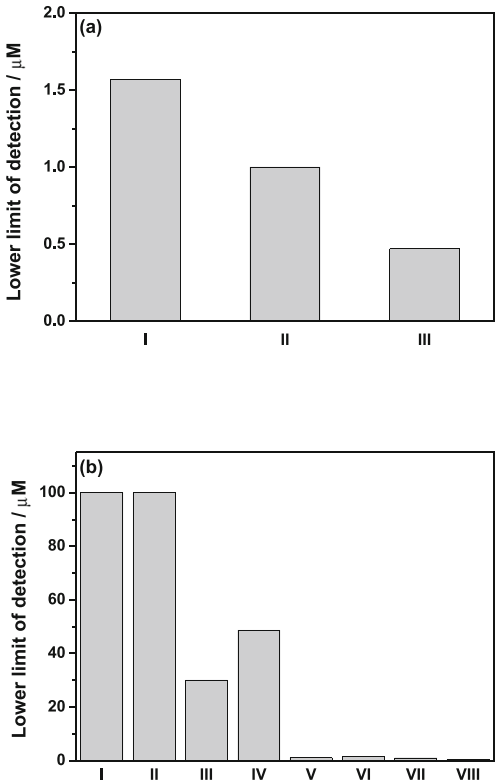

Fig. 4 (**a**) Histogram showing the lower limit of detection of pristine MWCNTs (*I*), P-MWCNTs (*II*), and N-MWCNTs (*III*) films towards $[Fe(CN)_6]^{3-/4-}$. (**b**) Comparison of lower limits of detection estimated in present work for carbon nanotubes composite films towards $[Fe(CN)_6]^{3-/4-}$ with those reported in literature for other novel composite films. The symbols are denoted as follows: CPE (*I*) [38]; CPE (*II*) [39]; GC (*III*) [40]; GC/MWCNTs (*IV*; *V*) [37]; MWCNTs (*VI*); P-MWCNTs (*VII*); N-MWCNTs (*VIII*)

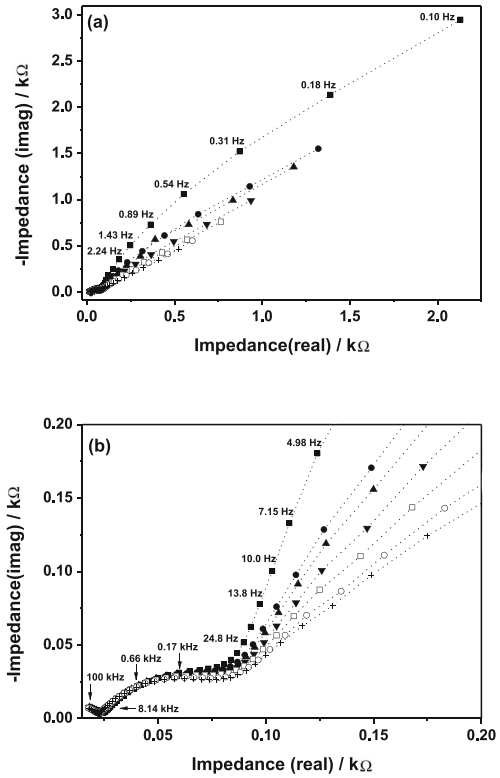

Fig. 5 (**a**) Representative EIS spectra recorded for various concentrations of $[Fe(CN)_6]^{3-/4-}$ (1.0 M KCl) on P-MWCNTs film in the frequency range from 0.1 Hz to 100 kHz at the half-wave potential of $[Fe(CN)_6]^{3-/4-}$ ($E_{1/2}$=+0.271 V vs. Ag/AgCl). (**b**) Zoom of EIS spectra in the high frequency range from 4.98 Hz to 100 kHz. The symbols are denoted as follows: 0.023 mM (*filled square*); 0.063 mM (*filled circle*); 0.091 mM (*filled upward triangle*); 0.118 mM (*filled downward triangle*); 0.167 mM (*open square*); 0.211 mM (*open circle*); 0.250 mM (*plus sign*)

the imaginary (Z_{imag}) impedance components. The type of recorded EIS spectra clearly reveals that the impedance is controlled by the interfacial electron transfer at high frequencies, while at low frequencies, the Warburg impedance is generated. Namely, the EIS spectra include a depressed semicircle at high frequencies, corresponding to the electron transfer limiting process (see zoom of EIS spectra in high-frequency region shown in Fig. 5b), and a linear part at low frequencies resulting from the diffusion limiting step of the electrochemical process. The extracted impedance data were satisfactorily fitted to the equivalent electrical circuit ($R_s+(C_{dl}/(R_{ct}+Z_w))$) (software Thales, version 4.15) (Fig. 6). The circuit elements are explained as follows: R_s represents the Ohmic resistance of electrolyte, R_{ct} is the charge-transfer resistance, C_{dl} corresponds to double-layer capacitance, and Z_w represents the Warburg diffusion impedance. The circuit used was found to fit satisfactorily the impedance data over the entire investigated frequency range (0.1 Hz–100 kHz) and the concentration range (0.032–0.250 mM). The mean and the maximum modified impedance errors resulted from the simulation process were estimated in all cases to be 0.3 and 2.5 %, respectively, which can be considered quite acceptable. It must be mentioned that in order to obtain satisfactory reproduction of

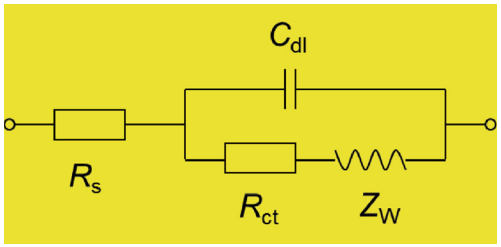

Fig. 6 Equivalent electrical circuit ($R_s+(C_{dl}/R_{ct}+Z_w)$) used for simulation of electrochemical impedance spectra recorded for $[Fe(CN)_6]^{3-/4-}$ (1.0 M KCl) on P-MWCNTs film (software Thales, version 4.15)

experimental impedance data, the capacitor was replaced by constant phase element. The explanation for the presence of constant phase element is the microscopic roughness of the surface of carbon nanotubes-based films that causes an inhomogeneous distribution in solution resistance and double-layer capacitance. The most suitable impedance parameter for further evaluation of the electrochemical features and for studying the interfacial properties of P-MWCNTs composite film is the charge transfer resistance (R_{ct}). This impedance parameter controls the electron transfer kinetics of redox system at electrode interface, and represents the barrier for the electron transfer process occurring onto electrode's surface. In other words, R_{ct} represents the hindering behavior of interface properties of the electrode, and it can be estimated from the diameter of capacitive semicircle in Nyquist plots [41]. As it can be seen in EIS spectra shown in Fig. 5b, the variation of concentration of electro-active species $[Fe(CN)_6]^{3-/4-}$ affects slightly the film's impedance behavior (the diameter of semicircle, and thus, the charge transfer resistance changes slightly with the variation of concentration). Namely, the findings demonstrate that the charge transfer resistance tends to increase slightly with the concentration of $[Fe(CN)_6]^{3-/4-}$ (in the range of 0.032–0.250 mM) implying that the barrier for electron transfer somewhat increases, and thus, the electron transfer rate (the kinetic of redox process) diminishes with rising concentration of electroactive compound. This observation is probably connected to the interruption of electron transfer process caused by the uncompensated resistance effect that becomes more significant with the increase of concentration of electro-active substance. The findings are in absolute agreement with the extracted CV-results, where a slight increase of ΔE_p, and thus, a decrease of k_s occurs with the increase of concentration of $[Fe(CN)_6]^{3-/4-}$. The estimated R_{ct} values for pristine MWCNTs, P-MWCNTs, and N-MWCNTs are included in Table 2. As it can be seen, the R_{ct} values tend to decrease with the following order: MWCNTs (50 Ω)>P-MWCNTs (35 Ω)> N-MWCNTs (17 Ω). The results demonstrate that the doping of carbon nanotubes diminishes the barrier for electron transfer, and thus, improves the kinetic of redox process taking place onto surface of nanotubes. Within the two different doping elements studied, nitrogen seems to improve better the electrocatalytic activity of nanotubes. The impedance results are in absolute agreement with those extracted by CV studies.

Namely, the kinetic parameter k_s estimated for $[Fe(CN)_6]^{3-/4-}$ onto carbon nanotubes composite films tends to increase with the following inverse order: MWCNTs<P-MWCNTs<N-MWCNTs, confirming that the charge-transfer resistance is inversely proportional to the exchange current, and thus, to heterogeneous electron-transfer rate constant [42].

Conclusions

In the presence work, novel P-MWCNTs composite films were fabricated by means of CVD technique with decomposition of TPP on oxidized silicon substrate using $FeCp_2$ as catalyst. The P-MWCNTs films were characterized using SEM, TEM, and Raman spectroscopy techniques. In addition, the novel P-MWCNTs composite films were electrochemically investigated with respect to their response to standard redox system $[Fe(CN)_6]^{3-/4-}$ (in the concentration range of 0.032–0.250 mM) in aqueous KCl solutions (1.0 M). For comparison reasons, electrochemical studies of $[Fe(CN)_6]^{3-/4-}$ onto pristine MWCNTs and N-MWCNTs were also carried out. The kinetics of redox process involving $[Fe(CN)_6]^{3-/4-}$ onto composite carbon nanotubes films tends to increase with the following order: MWCNTs<P-MWCNTs<N-MWCNTs. The sensitivity of the composite carbon nanotubes films towards $[Fe(CN)_6]^{3-/4-}$ enhances with the phosphorus doping (compared to pristine MWCNTs), but, however, the P-MWCNTs appear to be slightly less sensitive compared to N-MWCNTs. Specifically, the lower limit of detection of P-MWCNTs towards $[Fe(CN)_6]^{3-/4-}$ (LOD=1.0 μM) lies between the values of limit of detection obtained for pristine MWCNTs (LOD=1.57 μM) and N-MWCNTs (LOD=0.47 μM) composite films. Anyhow, the findings demonstrate that the novel P-MWCNTs film is rather sensitive compared to other novel films reported in literature, and consequently, it can be considered as quite suitable electrode in electrochemical sensing.

Acknowledgments The authors would like to thank Mrs. Doreen Schneider and Mrs. Sabine Heusing (Ilmenau University of Technology). The present research work was finally supported by Ilmenau University of Technology (project number: 6311, application number: 3002).

References

1. Bernholc J, Brenner D, Buongiorno Nardelli M, Meunier V, Roland C (2002) Annu Rev Mater Res 32:347
2. Matzui L, Ovsienko IV, Len TA, Prylutskyy Y, Scharff P (2005) Fullerenes Nanotubes Carbon Nanostruct 13:259
3. Mykhailenko O, Matsui D, Prylutskyy Y, Le Normand F, Eklund P, Scharff P (2007) J Mol Model 13:283
4. Ovsienko IV, Len TA, Matzui LY, Prylutskyy YI, Ritter U, Scharff P, Le Normand F, Eklund P (2007) Mol Cryst Liq Cryst 468:289
5. Lazarenko A, Vovchenko L, Matsui D, Prylutskyy Y, Matzuy L, Ritter U, Scharff P (2008) Mol Cryst Liq Cryst 497:397
6. Luo H, Shi Z, Li N, Gu Z, Zhang Q (2001) Anal Chem 73:915
7. Musamech M, Wang J, Merkoci A, Lin YH (2002) Electrochem Commun 4:743
8. Yu J, Zhao J, Hu C, Hu S (2007) J Nanosci Nanotechnol 7:1631
9. Xie X, Gan T, Sun D, Wu K (2008) Fuller Nanotub Carbon Nanostruct 16:103
10. Brahman PK, Dar RA, Tiwari S, Pitre KS (2012) Rev Anal Chem 31:83
11. Debnarayan J, Chia-Liang S, Li-Chyong C, Kuei-Hsien C (2013) Prog Mater Sci 58:656
12. Liu H, Zhang Y, Li R, Sun X, Abou-Rachid H (2012) J Nanoparticle Res 14:1016
13. Maciel IO, Campos-Delgado J, Cruz-Silva E, Pimenta MA, Sumpter BG, Meunier V, Lopez-Urias F, Munoz-Sandoval E, Terrones H, Terrones M, Jorio A (2009) Nano Lett 9:2267
14. Cruz-Silva E, Cullen DA, Gu L, Romo-Herrera JM, Munoz-Sandoval E, Lopez-Urias F, Sumpter BG, Meunier V, Charlier JC, Smith DJ, Terrones H, Terrones M (2008) ACS Nano 2:441
15. Cruz-Silva E, Lopez-Urias F, Munoz-Sandoval E, Sumpter BG, Terrones H, Charlier JC, Meunier V, Terrones M (2009) ACS Nano 3:1913
16. Szroeder P, Tsierkezos NG, Scharff P, Ritter U (2010) Carbon 48:4489
17. Tsierkezos NG, Szroeder P, Ritter U (2014) Microchim Acta 181:329
18. Tsierkezos NG, Ritter R (2010) J Solid State Electrochem 14:1101
19. Tsierkezos NG, Ritter R (2012) J Solid State Electrochem 16:2217
20. Tsierkezos NG, Wetzold N, Ritter U (2013) Ionics 19:335
21. Tsierkezos NG, Wetzold N, Ritter U, Hübler AC (2013) Monatsh Chem 144:581
22. Tsierkezos NG, Ritter U (2012) J Nanosci Lett 2:25
23. Tsierkezos NG, Wetzold N, Hübler AC, Ritter U, Szroeder P (2013) Sens Lett 11:1465
24. Tsierkezos NG, Ritter U (2011) Phys Chem Liq 49:729
25. Tsierkezos NG, Haj Othman S, Ritter U (2013) Ionics 19:1897
26. Ritter U, Scharff P, Siegmund C, Dmytrenko OP, Kulish NP, Prylutskyy YI, Belyi NM, Gubanov VA, Komarova LI, Lizunova SV, Poroshin VG, Shlapatskaya VV, Bernas H (2006) Carbon 44:2694
27. Ritter U, Scharff P, Dmytrenko OP, Kulish NP, Prylutskyy YI, Belyi NM, Gubanov VA, Komarova LA, Lizunova SV, Shlapatskaya VV, Bernas H (2007) Chem Phys Lett 447:252
28. Tuinstra F, Koenig J (1970) J Chem Phys 53:1126
29. Ferrari A, Robertson J (2000) Phys Rev B 61:14095
30. Szroeder P, Górska A, Tsierkezos N, Ritter U, Strupiński W (2013) Materialwiss Werkst 44:226
31. Wen YH, Zhang HM, Qian P, Zhou HT, Zhao P, Yi BL, Yang YS (2006) Electrochim Acta 51:3769
32. Nicholson RS, Shain I (1964) Anal Chem 36:708
33. Tsierkezos NG, Ritter U (2012) Phys Chem Liq 50:661
34. Gong K, Du F, Xia Z, Durstock M, Dai L (2009) Science 323:760
35. Tang Y, Allen BL, Kauffman DR, Star A (2009) J Am Chem Soc 131:13200
36. Tsierkezos NG, Ritter U (2012) J Solut Chem 41:2047
37. Perenlei G, Tee TW, Yusof NA, Kheng GJ (2011) Int J Electrochem Sci 6:520
38. Pandurangachar M, Swamy BEK, Chandrashekar BN, Gilbert O, Reddy S, Sherigara BS (2010) Int J Electrochem Sci 5:1187
39. Niranjana E, Swamy BEK, Naik RR, Sherigara BS, Jayadevappa H (2009) J Electroanal Chem 631:1
40. Hirano A, Kanai M, Nara T, Sugawara M (2001) Anal Sci 17:37
41. Peng H, Ma G, Mu J, Sun K, Lei Z (2014) J Mater Chem A 2:10384
42. Chirea M (2013) Catalysts 3:288